Pergamon

Cement and Concrete Research 31 (2001) 1487–1499

CEMENT AND CONCRETE RESEARCH

High-temperature behaviour of HPC with polypropylene fibres From spalling to microstructure

Pierre Kalifa[a,1], Grégoire Chéné[b,*], Christophe Gallé[c,2]

[a]*Centre Scientifique et Technique du Bâtiment, 24 rue J. Fourier, F-38400 St Martin d'Hères, France*
[b]*ISBA, Groupe ESIM, Technopôle Château Gombert, F-13451 Marseille cedex 20, France*
[c]*Commisariat à l'Energie Atomique, Bâtiment 158, F-91191 Gif sur Yvette cedex, France*

Received 17 January 2001; accepted 25 June 2001

Abstract

The addition of polypropylene (PP) fibres to high-performance concrete (HPC) is one way to avoid spalling of concrete under fire conditions. The present work contributes both to the understanding of the way in which fibres act and to optimising the fibre dosage. Pore pressure measurements performed on heated specimens showed that the presence of fibres led to a large decrease in the extent of the pressure fields that build up in the porous network during heating. This effect was also significant at dosages lower than the theoretical percolation threshold. These results are supported by permeability measurements carried out after various heat treatments and for various fibre dosages: they showed the striking effect of fibres from 200°C up, that is, very close to their melting temperature. The role of fibres is discussed through the analysis of concrete microstructure and fibre–matrix interactions as function of heat treatment.

Keywords: High-performance concrete; Polypropylene fibres; Temperature; Degradation; Permeability

1. Introduction

The sometimes-brittle behaviour of certain high-performance concretes (HPCs) under fire conditions may inhibit their use in buildings and tunnels. It was demonstrated that some HPCs may spall under certain thermal and mechanical stresses [1–12], and that the integrity of the structural element or of the structure itself may be jeopardised.

Spalling results from two concomitant processes: the so-called thermomechanical process, associated with the thermal dilation/shrinkage gradients that occur within the element when being heated [13,14], and the thermohydral process that generates high-pressure fields of gas (water vapour and enclosed air) in the porous network. The thermohydral process is controlled among several parameters by permeabilities to gas (vapour and air) and liquid. The permeability of HPC, being much lower than that of ordinary concrete and with the pressure built up with temperature, cannot be reduced [15,16].

Several experimental and theoretical works are being carried out to model spalling in order to predict the cases in witch the risk of spalling is high and to propose alternate solutions in terms of mix and element design. Technological solutions are also being developed to provide passive or active protection against spalling. Among them, the addition of polypropylene (PP) fibres in concrete appears to be very efficient [17–23]. PP melts at 170°C, whereas spalling occurs between 190°C and 250°C [10,24]. When melted and partially absorbed by the cement matrix, the fibres leave a pathway for gas. So they contribute to the creation of a network more permeable than the matrix, which allows the outward migration of gas and results in the reduction of pore pressure.

To our knowledge the literature reports only one building made of HPC with PP fibres (Japan Centre in Frankfurt, Germany [17]). However, other structures have adopted this solutions, especially in Japan and in the USA. The Japan Centre was made of concrete with nominal strength of 105

* Corresponding author. Tel.: +33-4-91-05-45-06; fax: +33-4-91-05-46-37.

E-mail addresses: quenard@cstb.fr (P. Kalifa), chene@isba.fr (G. Chéné), galle@cea.fr (C. Gallé).

[1] Tel.: +33-4-76-76-25-51; fax: +33-4-76-76-25-60.

[2] Tel.: +33-1-69-08-23-83; fax: +33-1-69-08-84-41.

0008-8846/01/$ – see front matter
PII: S0008-8846(01)00596-8

Table 1
Characteristics of PP fibres

Density at solid state [23]	0.93
Density at liquid state [23]	0.85
Thickness (μm)	50
Width (μm)	150
Length (mm)	19
Melting temperature (°C)	171
Temperature at vaporisation (°C)	341
Burning temperature (°C)	460
Thermal conductivity [23] (W/m K)	0.15

MPa, containing 2 kg/m^3 of PP fibres with a length of 12 mm and a diameter of 100–200 μm.

Several authors have studied the efficiency of organic fibres regarding spalling. Sarvaranta et al. [18] and Sarvaranta and Mikkola [19,20] showed that among various types of fibres, PP fibres were the most efficient. All other authors used PP fibres. The tests were conducted using standard thermal curves (close to ISO 834) on columns loaded [17,22] or not loaded [21,22,24], on small beams [23], on cylinders [21], and on small-size mortar plates [16–18]. The efficiency of fibres regarding spalling was in most cases estimated qualitatively through visual assessment of the degree of spalling. In Kalifa et al. [24], the columns ($30 \times 30 \times 120$ cm^3) were weighed during heating in order to measure the mass of concrete that was lost by spalling (besides water loss). The tests were performed on the same concrete used in the present study (average strength 105–110 MPa) and the fibre dosage ranged between 0 and 3 kg/m^3. It was shown that fibres had a good efficiency against spalling even at dosages as low as 0.9 kg/m^3 in the tested conditions. This result seems to be confirmed by Lennon and Clayton [23] although the results are not easy to analyse as presented. Sarvaranta et al. [18] and Sarvaranta and Mikkola [19,20] were the only ones who attempted a quantitative analysis by measuring the effect of fibre dosage on the rate of mass loss and on the shape of temperature curves: these parameters provide information of the way concrete evacuates water and gas. No significant fibre length effect was brought to light in these studies. However, Bentz [25] showed in a numerical study that for the same fibre dosage, longer fibres were more efficient. Also, the experimental studies did not quantify the effect of fibre dosage. They showed that fibres were efficient at dosages as low as 0.9 kg/m^3. From the industrial point of view, a dosage of 2 kg/m^3, a fibre length between 10 and 20 mm, and a fibre diameter of 50–200 μm are generally adopted rules for preventing current HPCs from spalling. However, these values are not optimised. Since the use of fibres significantly affects the workability of concrete, this optimisation is of significant interest. Also, these values cannot be extrapolated to higher range concretes (with higher strength, lower permeability, or lower grain size) without knowing exactly the way fibres act, in particular when they do not constitute by themselves a connected network, as at 0.9 kg/m^3.

The aim of the present work is to quantify the effect of PP fibres on the behaviour of concrete at high temperature and to understand the way fibres contribute to the creation of a network much more permeable than the plain matrix. The efficiency of fibres against spalling of a C110 column has been demonstrated in Ref. [24]. This efficiency is confirmed quantitatively in the present paper by measuring the effect of fibres on pressure and temperature fields in concrete blocks ($30 \times 30 \times 12$ cm^3) subjected to a unidirectional heat stress of lower severity than the ISO 834 curve. This is reported in Section 3. In order to understand the influence of fibres on these fields, permeability measurements and microstructure analysis were carried out after various heat treatments. This is addressed in Section 4. This study was conducted on the C110 mentioned above, with a fibre dosage ranging between 0 and 3 kg/m^3.

2. Materials

2.1. Polypropylene fibres

The PP fibres used have a length of 19 mm and a cross-section of 50×150 μm^2. The fibres are supplied in bunches that are dispersed at mixing. Their characteristics are gathered in Table 1. They melt at 171°C and turn into vapour at 341°C, as shown on the thermogravimetric (TGA) and differential thermal analyses (DTA) reported in Fig. 1. It is noticeable that they exhibit a slight dilation at melting (around 10%) [27].

2.2. Concrete

The C110 used in this work was studied in the French National Project BHP2000 under the name of M100 [28]. This concrete is made of calcareous aggregates, contains silica fume (10% of cement), and has a water-to-binder ratio of 0.3 (Table 2). The fibre dosage α_f ranges from 0 to 3 kg/m^3. In order to maintain a suitable workability of all mixes,

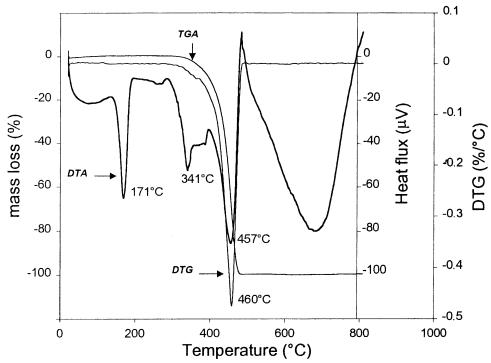

Fig. 1. DTA, TGA, and differential thermogravimetric analysis (DTG) of PP. The important points are the melting point (171°C), the vaporisation point (341°C), and the burning point (457°C).

Table 2
Mix design (kg/m^3)

Denomination	PTM	Permeability
Cement CPA CEM I 52.5 PM CP	415	415
Ground sand, Boulonnais, 0/5 mm (calcareous)	432	432
Seine sand, 0/4 mm (silicocalcareous)	439	439
Ground calcareous aggregate, Boulonnais, 5/12.5 mm	488	488
Ground calcareous aggregate, Boulonnais, 12.5/20 mm	561	561
Condensed silica fume	41.6	41.6
Superplasticizer Chryso GT	13.75	13.75
Water	139	139
Water-to-binder	0.3	0.3
PP fibres	0	
	0.5	0
	1.1	0.9
	1.75	1.75
	2.4	3
	3	

it appeared necessary to increase the amount of cement by 10% (38 kg/m^3) and the superplasticizer by 30% (3 kg/m^3).

The nominal compressive strengths measured on $\emptyset$ 16 cm $\times$ H 32 cm after 28 days in water are given in Table 3. The fibres have a small effect on strength: the latter decreases by a maximum of 8%. This decrease is probably due to the defects like air bubbles introduced at mixing.

3. Pore pressure, temperature, and mass loss

In this section, the thermohydral process that takes place in a concrete specimen during heating is analysed. Both quantitative and qualitative effects of fibres are studied.

3.1. Experimental

The experimental set-up that was developed for this test was described previously [10,26]. A thermal stress is imposed with the help of radiant heaters placed near the upper face of a prismatic specimen ($30 \times 30 \times 12$ cm^3), whereas the four lateral faces are heat-insulated. This set-up provides, therefore, a quasi-unidirectional solicitation in the central part of the specimen (Fig. 2).

The specimens are instrumented with pressure–temperature gauges that allow measuring pore pressure and temperature simultaneously at the same location. These gauges are made of a disk of porous sintered metal ($\emptyset$ 13 mm) encapsulated into a metal cup that is connected to a metal tube (Fig. 3). The pressure on both sides of the metal disk is that of the porous network. The free end of the tube sticks out of the rear face of the specimen. It is equipped with a tight connector that allows, firstly connecting the gauge to a piezoelectric pressure transducer, secondly to introduce a thermocouple down to the metal disk. Five gauges are placed in the 10×10 cm^2 central zone at 10, 20, 30, 40, and 50 mm from the heated face. Besides, the temperature of the heated face is measured by introducing a thermocouple in a plain tube placed in the concrete, with its extremity at 2 mm inward from the heated face.

All tests were carried out at heater temperature of 600°C during 6 h. This temperature was reached in a very short time. Two tests were performed for each mix.

After fabrication, the specimens were stored in a sealed bag for at least 3 months, therefore they had a homogeneous moisture state. The latter was measured on smaller specimens stored in the same conditions, by drying at 105°C until steady mass state (0.02% / 24 h). The initial moisture state ranged between 3.0% and 3.2% by mass.

3.2. Results and analysis

The three parameters, temperature field, pore pressure field, and mass loss, measured during these tests constitute three major indicators of the thermohydral process.

The establishment of the temperature field within the specimen is a function of the thermal properties of the material (which changes during heating due to microstructure changes [28]) as well as to the physical–chemical changes that occur during heating. The most energy-consuming transformation in the temperature range where spalling occurs (below 400°C) is water vaporisation.

As a corollary to the increase in temperature, the mass loss is mainly associated to water loss, transferred outwards in vapour state. The fibre mass fraction (up to 0.12%) is too low to significantly affect the specimen mass loss. Moreover, the loss of other cementitious components below 400°C is negligible [29]. The kinetics of mass loss is mainly controlled by the permeability of the concrete slice located between the heated face and the drying–dehydrating front.

Associated to these transfers of mass and energy is the build-up of a pressure field that passes through a maximum with time, which attests of the inward progression of a drying–dehydrating front [10,16]. This field is also mainly controlled by permeability to gas and liquid.

Our objective in this analysis is to assess the qualitative and quantitative influence of fibres on these parameters and if possible determine an optimal fibre dosage.

In Figs. 4 and 5, the mass loss and the rate of mass loss are represented as a function of time. These curves supply essential data for numerical simulation. Qualitatively, the most interesting information is supplied on Fig. 5: in the first part of the test, the rate of mass loss increases with

Table 3
Compressive strength after 28 days in water

Fibre dosage α_f (kg/m^3)	f_{c28} (MPa)
0	111.6 ± 4.5
0.5	112.0 ± 6.7
1.1	106.4 ± 3.1
1.75	102.6 ± 2.2
2.4	107.4 ± 1.0
3	105.4 ± 4.0

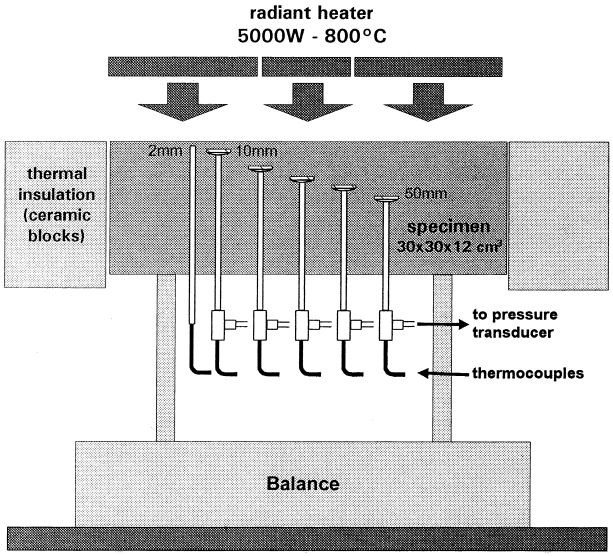

Fig. 2. PTM tests: the experimental set-up.

increasing fibre dosage. This effect is significant although it is largely attenuated by the fact that at a given time, the thickness of the zone affected by the drying–dehydrating process is low (typically 20 mm) with respect to that of the specimen (120 mm). The increase in the rate of mass loss with fibre dosage brings to light the contribution of the fibres in the creation of a connected network for the outward transfer of water. Similar observations were made by Sarvaranta et al. [18] and Sarvaranta and Mikkola [19,20] on mortar specimens with a smaller thickness (50 mm).

All specimens have a similar thermal behaviour (Fig. 6): at each depth, the global temperature rise does not depend on fibre dosage. Unpublished work showed that fibres had a low effect on the thermal properties of concrete. However, the temperature rise exhibits a plateau-like disturbance that starts above 100°C and ends between 160°C and 200°C, which is

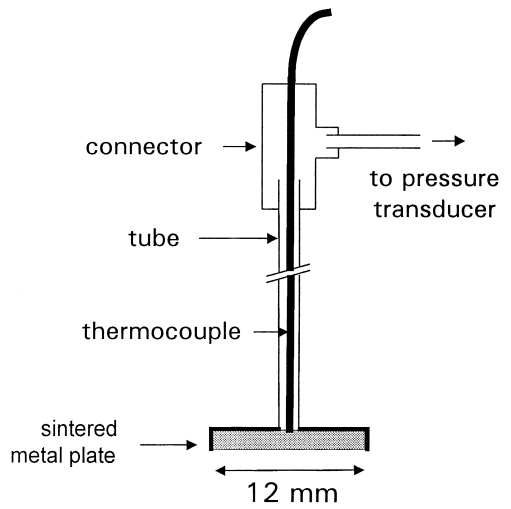

Fig. 3. Pressure–temperature gauge.

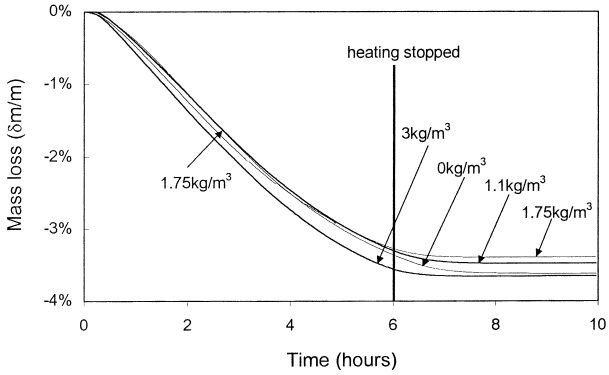

Fig. 4. PTM test: relative mass loss for various fibre dosages.

close to the melting point of the fibres. In the plain concrete, this disturbance ends around 250°C. It was previously demonstrated that this phenomenon is associated with the consumption of energy due to the vaporisation of water in the porous network, and that its end is correlated to the pressure peak, i.e., to the ingress of the drying–dehydrating front [10]. The presence of fibres when melted enables the water to be vaporised and expelled at a lower temperature. A careful analysis of the pressure curves also shows that the postpeak pressure drop is higher in fibre concrete. Once more, this shows the role of fibres in the creation of a network more permeable than the cement matrix.

The effect of fibres appears strikingly on Fig. 7: pressure-versus-time curves have a similar shape for all dosages, however, the height of the peaks drastically decreases with increasing fibre dosage. Hence, fibres directly contribute to the reduction of the stress fields in the skeleton due to pore pressure.

One also notices a rather high scattering of the curves, especially among the replicas. The latter may originate in concrete heterogeneity and in the presence of fibre clusters or in the creation of a macrocrack (e.g., at the matrix–pressure gauge interface) connected to the surface of the specimen.

The effect of fibre dosage is brought to light through three aspects of the pressure fields: the temperature reached

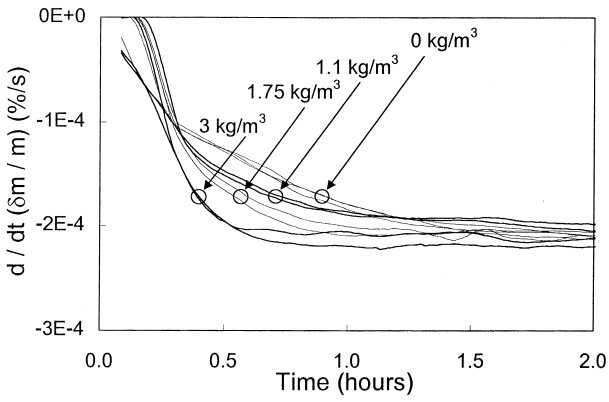

Fig. 5. Rate of mass loss versus time for various fibres dosages.

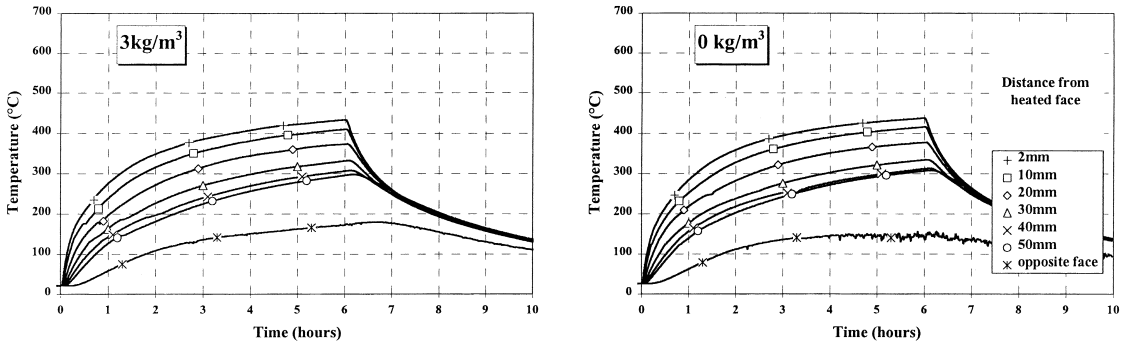

Fig. 6. Evolution of temperature with time at various depths for $\alpha_f = 0$ and 3 kg/m^3. Fibres do not affect the global thermal behaviour of the concretes.

at the peak ($T_{P_{max}}$), the amplitude of the peak (P_{max}), and the maximal pressure gradient $(\nabla P)_{max} = (\partial P/\partial x)_{max}$ where x is the depth. In order to reduce the effect of the data scattering, it was decided to consider for each fibre dosage, the four highest values of P_{max}, taken among the two replicas and without considering the depth. The average value and the standard deviation were calculated from these values. The corresponding values of $T_{P_{max}}$ were considered. The same procedure was applied to $(\nabla P)_{max}$.

The effect of fibre dosage on these three parameters is presented on Figs. 8–10. A significant decrease is noted in the parameters with increasing fibre dosage:

- $T_{P_{max}}$ increases from 180°C to 200°C for $\alpha_f = 3$ kg/m^3 to 240–260°C with no fibres. For $\alpha_f \geq 1.75$ kg/m^3, the pressure peak occurs at temperature very close to the melting point of the fibres. Therefore, it seems that fibres are effective as soon as they are melted.
- P_{max} increases from ≈ 1 MPa for $\alpha_f = 3$ kg/m^3 to $\approx$ 4 MPa for $\alpha_f = 0$ kg/m^3. For $\alpha_f = 1.1$ kg/m^3, P_{max} reaches about 2 MPa. For comparison, this value is very close to that reached in ordinary concrete [10].
- $(\nabla P)_{max}$ increases from 0.1 to 0.3 MPa/mm when α_f decreases from 3 to 0 kg/m^3.

One also notes that the effect of fibre dosage on $(\nabla P)_{max}$ and P_{max} barely changes for $\alpha_f \geq 1.75$ kg/m^3 or even 1.5 kg/m^3. This should be taken into consideration when designing a concrete mix with PP fibres.

In summary, these tests clearly bring to light the effect of fibres on the thermohydral process, especially on the pressure fields. Pressures peaks appear at a temperature close to the melting temperature of PP (171°C) and far below its temperature of vaporisation (341°C). It was mentioned earlier that PP dilates by about 10% when melting, which reduces the volume available for the transfer of gas and fluid. It is very unlikely that fibres can be evacuated from the specimen before the pressure peak, except for those with an end in contact with a free surface of the specimen.

The process through which the fibres contribute to the reduction of pore pressure is analysed in the next section, with the help of permeability measurements and microstructure characterisation.

4. Permeability and microstructure

In order for the PP fibres to contribute to a significant increase in permeability when melted, two criteria should be fulfilled. The first one is that, at least, part of the PP be absorbed by the surrounding cement matrix, so that a pathway for the transport of mass (liquid water, vapour, and gases) is created. This will be studied in Section 4.1. The second criterion is that the fibres constitute a connected network, either alone or with another population of defaults more permeable than the matrix itself. Garboczi et al. [30] studied the connection of ellipsoidal rigid objects randomly distributed in a volume and allowed to intersect. They carried out numerical simulations to calculate the proportion of objects at the percolation threshold as a function of their aspect ratio. The percolation threshold is the proportion of objects above which they constitute a connected network that crosses the considered volume of material. Above the percolation threshold, the transport property (here, permeability to gas) increases rapidly. Below the threshold, the property is very low and barely varies.

Let us identify the PP fibres (with a rectangular cross-section) to an ellipsoid with a length (l) of 19 mm and an unchanged cross-section surface area (7.5×10^{-3} mm^2). A fibre has therefore an equivalent diameter (d) of 98 μm and an aspect ratio ($\lambda = l/d$) of ≈ 200. After Garboczi et al. [30], the percolation threshold is then reached for fibre volume ratio of 0.32%. In this ratio, one should consider only the volume of the matrix, which is that of cement paste and sand, since the aggregate volume cannot be occupied by the fibres. In the mix used in this study, about 40% of the total volume are occupied by the aggregates. Therefore, the percolation threshold is reached for a fibre dosage of approximately 1.8 kg/m^3 of concrete. This value is within the range studied in this work. This theoretical prediction is very consistent with the experimental behaviour observed in the previous section: the dosages 1.75 and 3 kg/m^3 had a similar effect on pressure peaks. In other words, this would mean that as soon as fibres constitute by themselves a connected network, the latter is large enough to evacuate gases and vapour, thus to reduce pore pressure.

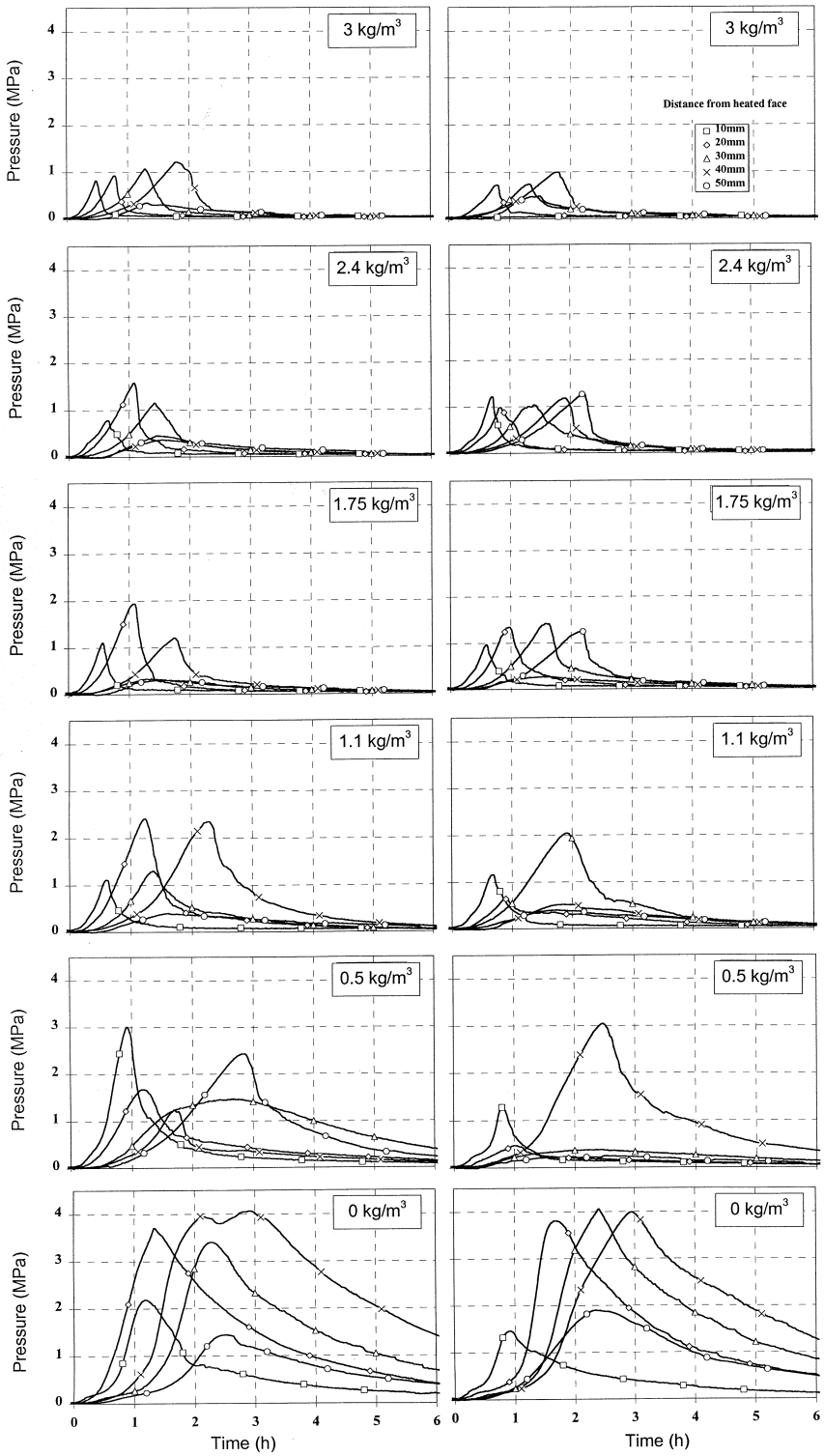

Fig. 7. Overview of the pressure fields for all tests. The striking effect of fibres on the span of the pressure peaks is brought to light.

However, fibres appeared to be prevented from spalling at dosages as low as 0.9 kg/m^3, which is far from the percolation threshold. Also, the distribution of fibres in the concrete may not be very homogeneous, so that the effective percolation threshold is probably reached at a fibre dosage higher than the theoretical value. Therefore, the connected network that enables to significantly increase concrete permeability is obtained at dosages higher than the percolation threshold, which means that this network is not constituted with the fibres. This question is addressed in the following.

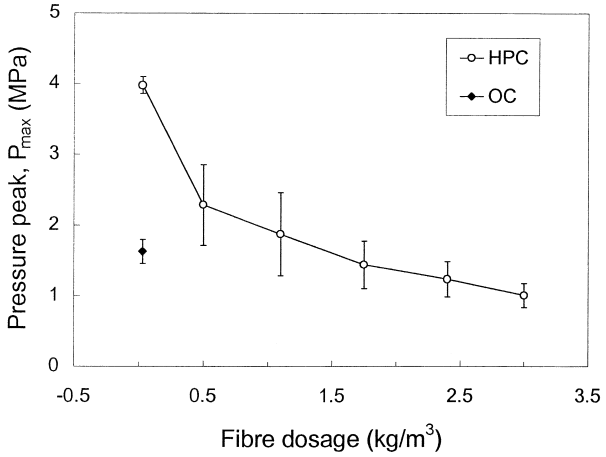

Fig. 8. Pressure peaks versus fibre dosage.

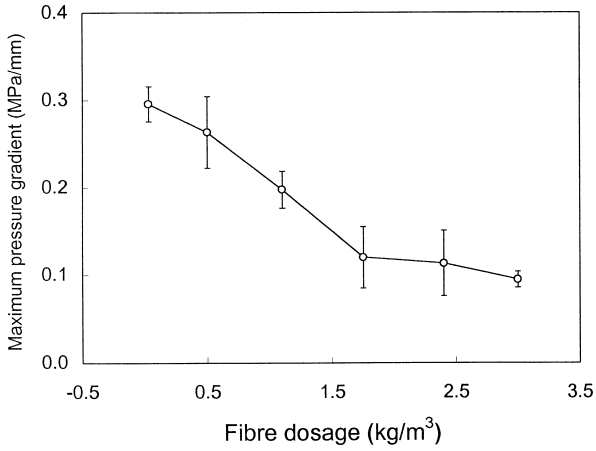

Fig. 10. Maximum pressure gradients versus fibre dosage.

4.1. Microstructure and fibre–concrete interactions

In order to understand the role of fibres, the evolution of concrete porosity is studied as well as the interactions between melted PP and cement matrix.

4.1.1. Water porosity

Water porosity measurements were performed on concrete containing 0, 0.9, 1.75, and 3 kg/m^3. The specimens are halves of $\emptyset$ 11-cm $\times$ H 5-cm slices cured for 3 months in sealed bags. Before measurement, the specimens were submitted to the following heat treatment: they were heated at 1°C/min up to a target temperature of 200°C, 300°C, and 400°C, respectively. This temperature was maintained for 6 h, then it was decreased to 23°C at a rate of 1°C/min. The duration of the plateau was meant to ensure that steady mass state was reached. The porosity measurements provide residual values. Besides, a series of specimens was maintained firstly at 80°C in a ventilated chamber until steady mass state, which was defined as a mass variation $\partial(\delta m/m)/\partial t$ lower than 0.02%/24 h. Porosity measurement was performed at that stage, then these specimens were dried at 105°C and a new porosity measurement was performed. In most cases, three specimens were tested for each condition. Porosity (ε) was measured according to a procedure described in Ref. [28], which is very close to that of the ISO 5017:1988 standard. ε is calculated using the relationship:

$$\varepsilon = \frac{m_{sat} - m_T}{m_{sat} - m_{sat}^{imm}} \times 100$$

where m_{sat} and m_{sat}^{imm} are the mass of the saturated specimen measured in air and in water, respectively. Specimen saturation was obtained by leaving the specimen under vacuum for 24 h before immersing it into water. m_T is the mass of the specimen after heat treatment.

Porosity results are displayed on Fig. 11 as a function of heat treatment and fibre dosage. A rapid increase in the accessible pore volume is observed between 80°C and 105°C. This is mainly due to the withdrawal of free or physically bound water that could not be withdrawn at 80°C. It does not correspond to a significant alteration of the matrix itself. Between 105°C and 400°C, the increase in porosity is lower, although it increases with fibre dosage: this increase ranges from 0.7% in plain concrete (consistent with Ref. [28]) to 2% for $\alpha_f = 3$ kg/m^3.

In any case, the increase in the porous volume due to heat treatment is rather low, contrary to permeability (see Section 4.2).

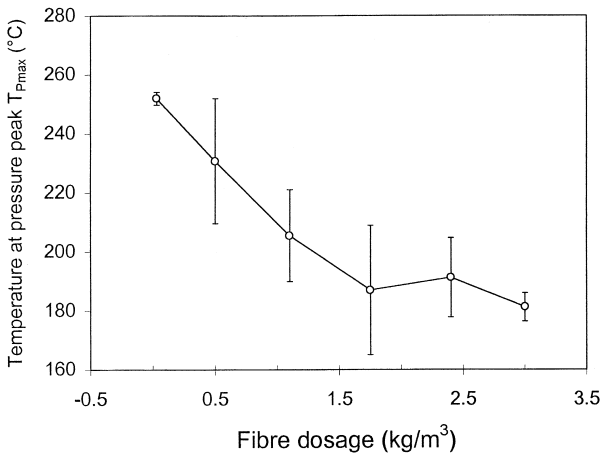

Fig. 9. Temperature at pressure peak versus fibre dosage.

4.1.2. Microcracking

Observations of the microcrack population were carried out with an optical microscope on concrete surfaces impregnated with a fluorescent resin and polished. These surfaces were taken from the $\emptyset$ 11-cm $\times$ H 22-cm specimens that were used for the permeability measurements (see Section 4.2). The surfaces were lit with ultraviolet light and observed through a polarising filter so that the fluorescent

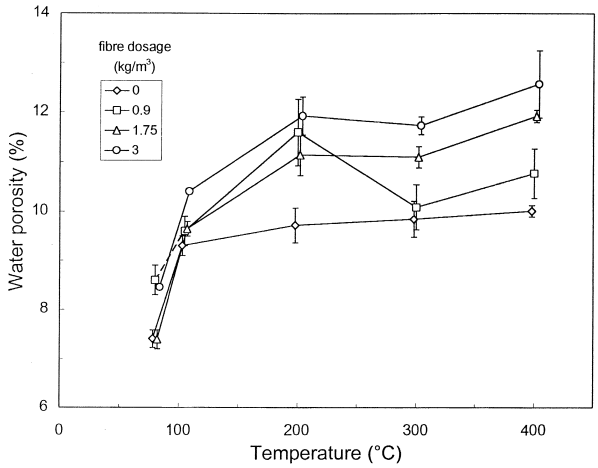

Fig. 11. Water porosity versus heat treatment and fibre dosage.

resin that penetrated into the defaults was easily distinguished from the rest of the concrete. This procedure was described in Ref. [29]. The concretes that were studied are without fibres at 400°C and with $\alpha_f = 3$ kg/m^3 at 200°C, 300°C, and 400°C. The procedure for heat treatment was that described in Section 4.1.1.

The most interesting and surprising aspect of these observations stems from the comparison between the two concretes at 400°C: the fibre concrete exhibits a much higher crack density than the plain concrete, as shown on Fig. 12. In the fibre concrete, cracks are very thin (close to 1 μm) and form a dense network between and around the sand and aggregate skeleton. On the other hand, in the plain concrete, cracks are thicker (around 10 μm) and cover a large distance by linking the bigger aggregates.

The reason why these concretes behave in such different way regarding cracking has not been elucidated yet. Microcracking in heated concrete results mainly from the thermal dilation/shrinkage gradients between the cement and the aggregates. In the studied temperature range, aggregates dilate whereas the paste shrinks as a result of dehydration. It is assumed that the fibre beds help the nucleation of cracks locally as they have sharp angles. Thus they favour the distribution of microcracking. Another cause of this difference may be that fibres slightly dilate at melting, thus creating a tensile stress in the matrix, which could help nucleating cracks. These hypotheses should be confirmed.

The second significant aspect is that crack density is much higher at 400°C than at 200°C, even 300°C. The same observations were made on plain HPC by Tsimbrovska [34]. Let us remember that the state of the microstructure at 200°C is of most interest for our study since pressure peaks occurred between 180°C and 250°C.

4.1.3. Fibre–matrix interactions

In order to study the behaviour of fibres after melting, observations with a scanning electron microscope (SEM) were done on polished surfaces taken from the core of $5 \times 5 \times 10$ cm^3 concrete specimens that were exposed to a temperature ranging between 160°C and 200°C for at least 6 h. These observations showed that as soon as temperature exceeds the fibre melting point (171°C) the fibres are not visible anymore in their initial bed (Fig. 13). This brings out that the polymer was absorbed by the porous network despite the large size of the molecules compared to pore diameter.

This statement was confirmed using the simple "water drop" test according to the following procedure. A very thin

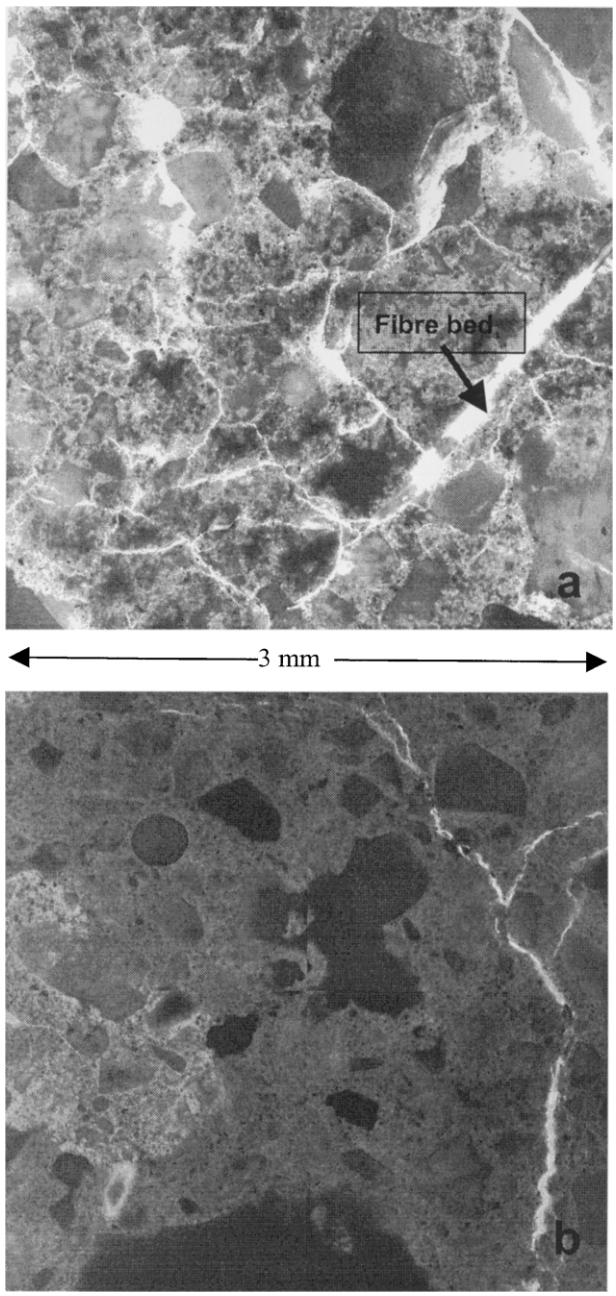

Fig. 12. (a) Fibre concrete ($\alpha_f = 3$ kg/m^3) and (b) plain concrete after 400°C treatment. The images represent a polished surface impregnated with fluorescent resin and observed under blue and polarised light. Cracks and fibres filled with the resin appear in white. These pictures clearly show the difference in damage between fibre and plain concrete.

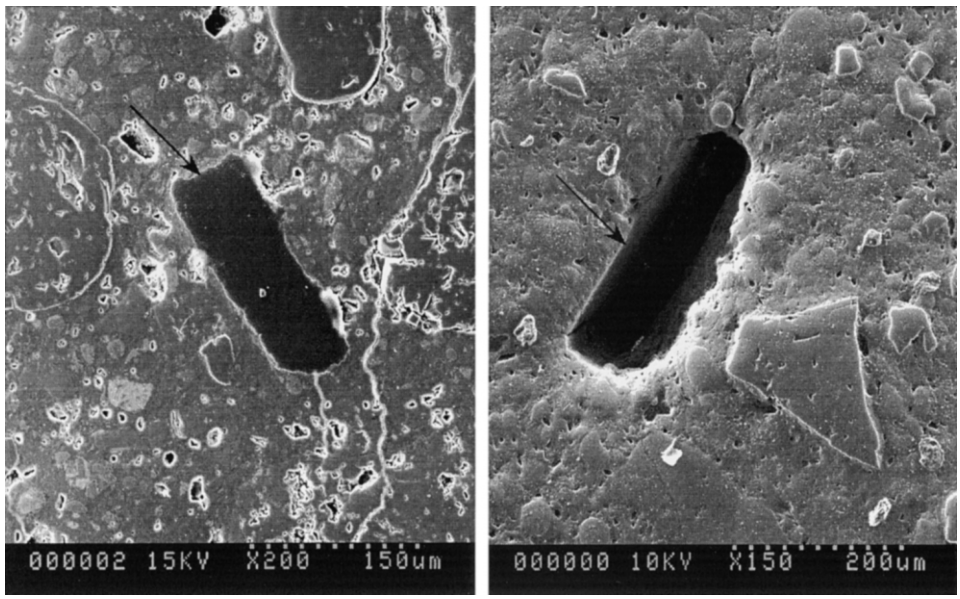

Fig. 13. Cross-section of a fibre observed through an SEM. The fibre is visible at initial state (left) but the polymer disappeared after a 200°C treatment (right) and only the fibre bed is visible.

layer of fibre was placed on a ground surface of concrete on an area of about 4 cm^2. A 2-cm edge cube was then placed on the fibres in order to keep them in contact with the concrete surface (Fig. 14). This set-up was heated up to a temperature ranging between 170°C and 200°C with a heating and cooling rate of 1°C/min. After cooling, the concrete cube was removed, a water drop was placed on fibre site, and the behaviour of the droplet was observed. The results are as follows: after 170°C exposure, the drop stayed in place, which means that the melted fibres had made an impermeable layer on the concrete surface. At 180°C and above, the drop was absorbed by the concrete, however much slower than on virgin concrete. This means that the polymer had actually penetrated the porous network, and decreased the rate of water absorption. This very simple experiment shows qualitatively that the cement matrix is able to absorb the melted PP, thus creating a new pathway for liquid water, vapour, and gas.

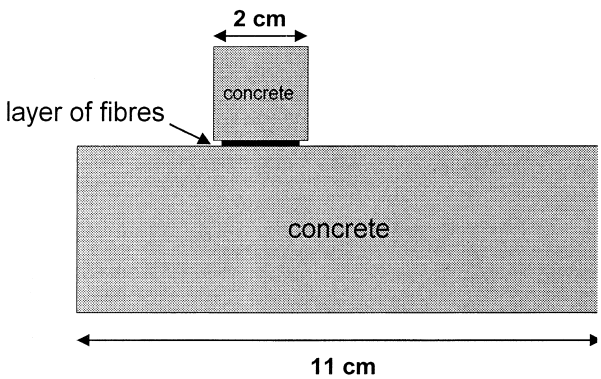

Fig. 14. Schematic of the water drop test.

4.2. Intrinsic permeability of fibre concrete

4.2.1. Experimental

The experimental conditions for permeability measurements (fibre dosages, curing conditions, heat treatments) were the same as those for porosity measurements (except for the 105°C heat treatment that was not considered). The measurements were also performed after cooling, therefore they provide residual values. The specimens were taken from $\emptyset$ 11 cm $\times$ H 22 cm.

For permeability measurements on plain concrete and on fibre concrete heated at 80°C, the standard Cembureau permeameter was used [31], and specimens were 50 mm thick. This apparatus could not reasonably be used on fibre concrete for $T \geq 200$°C: due to the length of the fibres (19 mm), the specimens were smaller than the representative volume. For this reason, the tests were performed using a Hassler permeameter [32] on $\emptyset$ 11-cm $\times$ H 20-cm specimens. This apparatus is also a constant-charge permeameter with a maximum input pressure of 5 MPa. The maximum pressure applied was around 1 MPa. For sake of comparison, tests were done on both permeameters for fibre concrete at 80°C and plain concrete at all other temperatures.

In all cases, the intrinsic permeability was determined using the Klinkenberg method [33]: permeability to nitrogen (K) was measured for various pressure gradients and the intrinsic permeability (k) was calculated by linearly extrapolating to infinite pressure, the line $K = f(1/\bar{P})$:

$$K = k\left(1 + \frac{b}{\bar{P}}\right)$$

where $\bar{P}$ is the average pressure and b is a coefficient determined experimentally.

4.2.2. Results and analysis

Row values of intrinsic permeability are displayed versus temperature and fibre dosage on Fig. 15. A low data scattering is noted. For this reason, only averages will be considered in the following analysis. Also, the results obtained on plain concrete are very close to those of Tsimbrovska et al. [29] on similar concrete. The following trends appear in this graph.

• At 80°C, the two permeameters yield very similar results. It is not quite the case at higher heat treatments: measurements performed with the Hassler permeameter yield higher values than those with the Cembureau one. The reason of this discrepancy lays probably not in the method of measurement, but rather in the difference in specimen size: the bigger specimens undergo larger thermal gradients at heating and cooling, which may induce larger cracking. However, this permeability difference is rather small compared to permeability changes with heat treatment.

• Fibre concretes have the same permeability at 80°C, which is only two times larger than that of plain concrete. The addition of fibres, therefore, poorly influences the initial structure of the porous network regarding permeability.

• At 200°C, fibre concretes exhibit a much larger permeability increase than the plain concrete. For comparison, at this temperature, the permeability for $\alpha_f = 0.9$ kg/m^3 is close to that of an ordinary concrete after the same heat treatment, as measured previously [9].

The effect of fibres on permeability is better brought to light on Fig. 16, which gives permeability $k(T)$ normalised to that at 80°C, $k(80)$, as a function of fibre dosage and heat treatment. In the log-normal diagram, the plain concrete exhibits a quasi-linear increase with temperature. Tsimbrovska et al. [29] and Tsimbrovska [34] showed that with the help of mercury intrusion porosimetry measurements this increase is associated with two main changes in the microstructure. Between 80°C and 300°C, the main factor is the increase in pore size: the monomodal pore size distribution shifts towards larger pores. From 300°C up, especially

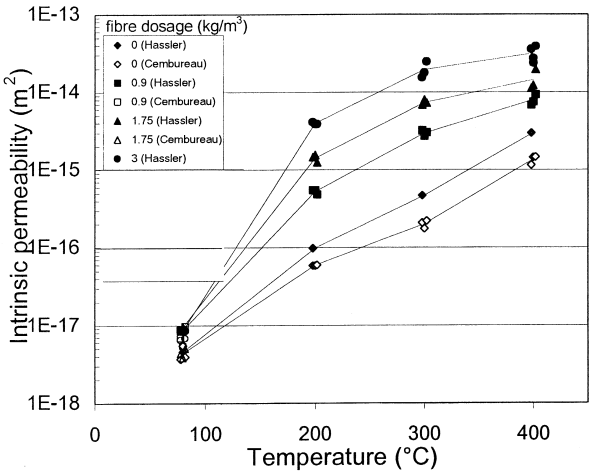

Fig. 15. Intrinsic permeability versus temperature and fibre dosage.

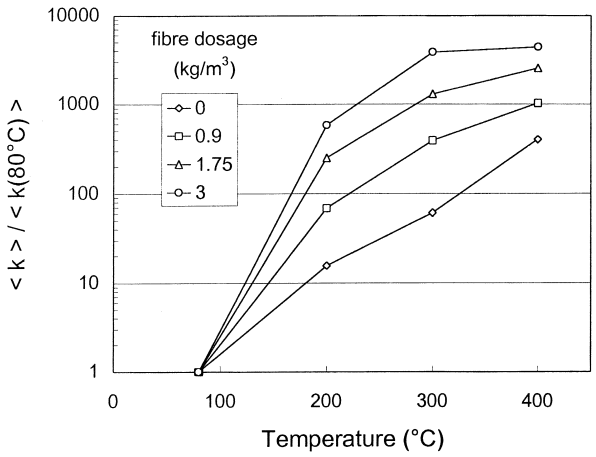

Fig. 16. Intrinsic permeability normalised to that at 80°C (averages), $k(T)/k(80°C)$, versus temperature and fibre dosage.

at 400°C, permeability is mainly controlled by cracking, as observed in the previous section.

Fibre concretes show a completely different behaviour: permeability follows a logarithmic type progression with temperature. This tendency is most marked for $\alpha_f = 3$ kg/m^3: k is multiplied by about 600 between 80°C and 200°C, whereas this factor is reduced to 7 between 200°C and 300°C. This means that the increase in permeability is mainly controlled by the fibres as soon as they are melted. Therefore, the slope of the segment would be even steeper if we had made a measurement at just below fibre melting (e.g., 150°C). The shape of the curve is the same for other dosages, but the tendency is less marked.

The most spectacular way to bring to light the contribution of fibres to permeability is shown on Fig. 17 where the ratio $\beta = k$(fibre concrete)/k(plain concrete) is plotted versus temperature and fibre dosage. This ratio reveals the relative contribution of fibres to permeability with respect to that of the matrix. For $\alpha_f = 3$ kg/m^3, β reaches a maximum of 85 at 200°C, decreases slightly at 300°C then decreases strongly to 20 at 400°C. In other words, the relative contribution of fibres

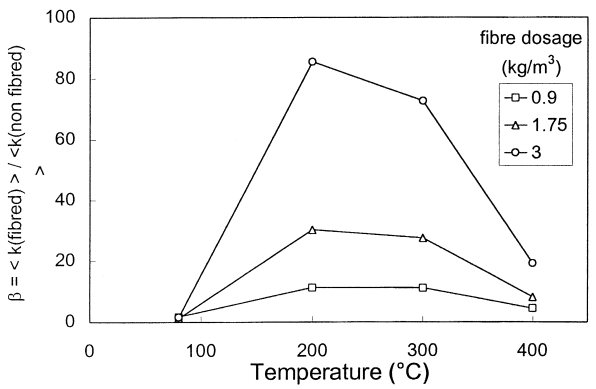

Fig. 17. Intrinsic permeability of fibre concretes normalised to that of plain concrete (averages) versus temperature and fibre dosage.

to permeability is much higher at 200°C (which is where the pressure peak occurs) than at 400°C. The same tendency stands for other dosages however with a lower span.

4.3. Discussion

The permeability measurements brought to light the major role of fibres as soon as they are melted, in the creation of a connected network for the transfer of fluids. This role decreases with decreasing fibre dosage. However, it is still significant at dosages lower than the percolation threshold estimated by Garboczi et al. [30].

It was demonstrated that flow uses the largest and straightest path (which is the better connected and less tortuous one) [35–37]. Permeability is controlled by the smallest link of this connected path. Many representations were elaborated using the electrical analogy to model heat and mass transport in porous media [38–43]. The porous network is then identified to a complex combination of elements in series and/or in parallel. For a correct representation of the medium taking into account its topography, these models often use fitting parameters determined experimentally. However, they are of great help for a semiquantitative analysis.

In order to understand qualitatively the relative contributions to mass transport of the concrete phases and fibres, let us consider the transport network as a three-phase system.

• *The fibres:* They melt at 171°C and are partially or totally absorbed by the porous network of the cement matrix. They leave a channel with a length of 19 mm and an equivalent diameter lower than 98 μm. These dimensions are much larger than those of the other defaults of the composite. The fibre beds therefore constitute a preferential pathway.

• *The porous network of the cement matrix and the interfacial transition zones (ITZ):* The global volume of pores poorly increases with temperature (from 0.7% to 2% between 105°C and 400°C, depending on fibre dosage). The pore size distribution is characterised by a peak that broadens towards larger size as temperature increases [29]. Although ITZs are very thin in HPCs, they constitute the weakest link of the matrix regarding permeability, whether they are cracked or not.

• *The crack population:* Significant cracking was detected from 300°C up, but not at 200°C. Fibres significantly influence the characteristics of the crack population: in particular, crack density is much higher at higher fibre dosage.

The relative contribution of each phase described above is a function of fibre dosage on the one hand, temperature on the other hand. Two main cases should be considered:

• *Fibre dosage is high*, so that fibres alone constitute a connected network. This is probably the case for $\alpha_f \geq 1.75$ kg/m^3. The transport network may be identified to a combination of two elements in parallel (Fig. 18a): (i) fibres and (ii) the system (pores + ITZs + cracks). The latter is also a serial/parallel combination of its components. At 200°C, the preferential pathway for gases and liquids is the connected network left by the fibres that were melted and partially or totally absorbed by the matrix. According to our observations, the matrix was barely altered and its contribution is low. On the contrary, the latter increases at higher temperature as a result of changes in the microstructure: increase in porosity, average pore size, and above all, strong increase in crack density. As a result, the ratio β decreases from 80 to 20.

• *Fibre dosage is lower*, so that fibres alone do not constitute a connected network. This is certainly the case for $\alpha_f < 1.75$ kg/m^3. Fibres are linked to each other through the matrix. Then the parallel system of the previous case becomes more complex (Fig. 18b): fibres do not intervene alone but in series with the matrix. The efficiency of the fibres then depends on the state of the microstructure. At 200°C, very few cracks were spotted in the matrix or at the ITZ. The changes in microstructure lay mainly in an increase in porous volume and in average pore size. This is the reason why for $\alpha_f = 0.9$ kg/m^3, β is only 11. However, to identify the efficient transport network, one should consider that fibre length (19 mm) is very close to that of the bigger aggregate size (20 mm). As a result, the probability for fibres to touch two aggregates is very high, thus their ITZs are connected. Therefore, the combined ITZ/fibre percolation may be the primary mechanism at that temperature.

At higher temperatures, the porous network becomes more permeable and crack density increases. As a result, the efficiency of the fibres increases and also that of the matrix too. At 400°C, when the crack population forms a connected network by itself, the relative contribution of fibres and β decreases (Fig. 17).

This short analysis shows that the use of an electrical analogy for representing the transport network provides a fairly good tool for explaining qualitatively the evolution of permeability with temperature, as observed experimentally. However, the hypotheses made should be confirmed by numerical simulation. This is currently being done at NIST (USA).

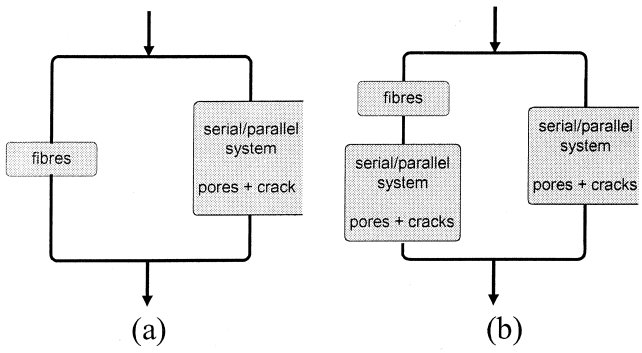

Fig. 18. Electrical analogy for representing mass transport through fibre concrete: (a) when fibres constitute by themselves a connected network and (b) when fibres do not constitute by themselves a connected network.

5. Summary and conclusions

The experimental work presented in this paper was based on the fact that PP fibres have been used in HPC constructions at a dosage of 2 kg/m^3 with the intention of reducing the propensity of concrete to spall, but that very few studies were carried out to understand the physical process through which fibres act against spalling, and to optimise the fibre dosage. Besides, fire tests carried out on columns and reported elsewhere showed that fibres had a significant effect at dosages as low as 0.9 kg/m^3, which is far below the theoretical percolation threshold.

The PTM tests carried out on fibre HPCs showed that fibres have a striking effect on the pressure fields that built up in the porous network during heating: as fibre dosage increased from 0 to 3 kg/m^3, pressure peaks were reduced by a factor of 4 and pressure gradients were reduced by a factor of 2. These effects were mostly pronounced between 0 and 1.75 kg/m^3 and less pronounced between 1.75 and 3 kg/m^3. Considering the theoretical work by Garboczi et al. [30], this change in fibre effect around 1.75 kg/m^3 may be related to the fact that fibres have reached the percolation threshold at that dosage.

The permeability measurements carried out after various heat treatments and for various fibre dosages supported the results of the PTM tests. They showed the striking effect of fibres from 200°C up, which is very close to their melting temperature: for a dosage of 3 kg/m^3, the intrinsic permeability (k) increased by a factor of 600 between 80°C and 200°C; at 200°C, k increased 85 times as fibre dosage increases from 0 to 3 kg/m^3. At that temperature, the melted PP cannot be evacuated. The polymer is certainly absorbed by the surrounding matrix, partially or totally, as brought to light by the simple droplet test that was carried out, as well as by SEM observations. The rapid increase in permeability with temperature enables the evacuation of vapour and gases, thus releasing the pressure. Complementary permeability measurements should be performed between 100°C and 170°C in order to assess the role of fibres before they melt.

The relative contribution of fibres to mass transport decreased at 400°C, as a result of the evolution of the microstructure: slight increase in porosity and above all microcracking. The latter appeared to be significantly influenced by the presence of fibres: at 3 kg/m^3, microcracking was characterised by a higher density and by smaller cracks than in plain concrete. A satisfactory explanation of this phenomenon was not found yet. It may have a significant effect on spalling as it may change the local stress distribution. Further microstructure analysis should be done between 100°C and 170°C.

Fibres have a significant effect on both pressure and permeability even at dosages lower than the theoretical percolation threshold. Using an electrical analogy to simulate the evolution of permeability with fibre dosage and temperature, it was shown that fibres act in a serial/parallel system with pores, ITZs, and cracks when they are formed. This model should be confirmed by numerical simulation.

As a conclusion, it appears that the fibre dosage of 2 kg/m^3 with a fibre length in the order of 20 mm is an efficient solution for preventing spalling in HPC up to 100 MPa under ISO 834 conditions. However, this dosage could certainly be reduced because it may not be necessary to reach (or even exceed) the fibre percolation threshold. Pressure measurements as well as permeability measurements suggest that a dosage around 1 kg/m^3 should be sufficient for this type of concrete and this range of heat solicitation. This may not apply to other types of concrete, with other aggregate size distribution or with greater pore refinement, as in UHPC, in which the percolation threshold is probably at a minimum. This area should be studied in the future. Also, PTM tests and microstructure analysis should be carried out in more severe heating conditions (close to that of standard fire curves) in order to assess the effect of heating kinetics.

Acknowledgments

The authors would like to acknowledge the French National Project BHP2000 that partially funded this work. They are also grateful to Dale Bentz (NIST) who contributed to the development of the study through fruitful exchanges.

References

[1] K. Hertz, Heat-induced explosion of dense concretes, Institute of Building Design Report No. 166, Technical University of Denmark, 1984.
[2] A. Noumowe, P. Clastres, G. Debicki, M. Bolvin, Effect of high temperature on high performance concrete (70–600°C) — Strength and porosity, in: V.M. Malhotra (Ed.), Third CANMET/ACI International Conference on Durability of concrete, Nice, France, 1994, pp. 157–172.
[3] U. Diederichs, U.-M. Jumppannen, V. Penttala, Behaviour of high strength concrete at high temperatures, Espoo 1989, Report 92, Department of Structural Engineering, Helsinki University of Technology, 1992, pp. 15–26.
[4] D.E. Allen, T.T. Lie, Fire resistance of reinforced concrete columns and walls, in: NRCC (Ed.), Proceedings of Canadian Structural Concrete Conference, Ottawa, Canada, June 1977, pp. 17–33.
[5] L.A. Ashton, S.C.C. Bate, The fire-resistance of prestressed concrete beams (Paper No. 6444)T. Telford (Ed.), Proc. Inst. Civil Eng., London 17.
[6] J.-J. Jensen, E.A. Hansen, U. Danielsen, S. Seglem. Offshore concrete structures exposed to hydrocarbon fire, in: University of Edinburg (Ed.), the First International Conference on Concrete for Hazard Protection, Edinburg, UK, 1987, pp. 147–149.
[7] G. Sanjayan, L.J. Stocks, Spalling of high strength silica fume concrete in fire, ACI Mater. J. 90 (2) (1993) 170–173.
[8] I.W.J. Copier, The spalling of normalweight and lightweight concrete on exposure to fire, Heron 24 (2) (1979) 3–92.
[9] P. Kalifa, M. Tsimbrovska, Comportement des BHP à hautes températures, état de la question et résultats expérimentaux, Cah. CSTB (1998) 3078, pp. 1–16.
[10] P. Kalifa, F.D. Menneteau, D. Quenard, Spalling and pore pressure in HPC at high temperatures, Cem. Concr. Res. 30 (2000) 1–13.

[11] F.A. Ali, R.J. Connolly, P.J.E. Sullivan, Spalling of high strength concrete at elevated temperature, Appl. Fire Sci. 6 (3) (1996–1997) 3–14.
[12] P.J.E. Sullivan, Deterioration and explosive spalling of high strength concrete at elevated temperature, in: D. Naus, Rilem Publications (Eds.), Proceedings of the International RILEM Workshop on Life Prediction and Aging Management of Concrete Structures, Cannes, France, 2000.
[13] F.J. Ulm, O. Coussy, Z.P. Bazant, The "Chunnel" fire: I. Chemoplastic softening in rapidly heated concrete, J. Eng. Mech. 125 (3) (1999) 272–282.
[14] Z.P. Bazant, M.F. Kaplan, Concrete at High Temperatures. Material Properties and Mathematical Models, Longman, Burnt Mill, England, 1996.
[15] T.Z. Harmathy, Effect of moisture on the fire endurance of building element, Research Paper No. 270, Division of Building Research, National Research Council, Ottawa, Canada, 1965.
[16] Y. Anderberg, Spalling phenomena of HPC and OC, in: L.T. Phan, N.J. Carino, D. Duthinh, E. Garboczi (Eds.), Proceedings of International Workshop on Fire Performance of High-Strength Concrete, NIST, Gaithersburg, MD, USA, 1997, pp. 69–73.
[17] R. Breitenbücker, High strength concrete C 105 with increased fire resistance due to polypropylene fibres, in: F. de Larrad, R. Lacroix (Eds.), 4th International Symposium on the Utilization of High-Strength/High-Performance Concrete, Paris, France, 1996, pp. 571–577.
[18] L. Sarvaranta, E. Jarvela, E. Mikkola, Fibre mortar composites under thermal exposure, in: Pluralis (Ed.), Proceedings of 2nd International Symposium on Textile Composites in Building Construction, Lyon, France, 23–25 June 1992, pp. 47–56.
[19] L. Sarvaranta, E. Mikkola, Fibre mortar composites in fire conditions, Fire Mater. 18 (1994) 45–50.
[20] L. Sarvaranta, E. Mikkola, Fibre mortar composites under fire conditions: Effects of ageing and moisture content of specimens, Mater. Struct. 27 (1994) 532–538.
[21] A. Nishida, N. Yamazaki, H. Inoue, U. Schneider, U. Diederichs, Study on the properties of high strength concrete with short polypropylene fibers for spalling resistance, in: K. Sakai, N. Banthia, O.E. Gjorv (Eds.), Proceedings of the Symposium on Concrete Under Severe Environment 2, 1995, pp. 1141–1150.
[22] U. Diederichs, U.M. Jumppanen, U. Schneider, High temperature properties and spalling behaviour of high strength concrete, 4th Int. Workshop on High Performance Concrete — Characteristics, Material Properties and Structural Performance, Weimar, Germany, October 5–6, 1995.
[23] T. Lennon, N. Clayton, Fire tests on high grade concrete with polypropylene fibres, BRE Report 395, 1999.
[24] P. Kalifa, D. Pardon, P. Pimienta, Comportement au feu de BHP additionnés de fibres de polypropylène, Cah. CSTB, (Sept., in press).
[25] D. Bentz, Fibers, percolation and spalling of high performance concrete, ACI Mater. J. 97 (3) (2000) 351–359.
[26] P. Kalifa, F.D. Menneteau, Mesures de pression, température et perte en masse dans les bétons à hautes températures, mise au point d'une métrologie originale, Cah. CSTB 3154, 1999, pp. 1–17.
[27] Polymer Handbook, second ed., 1974.
[28] P. Kalifa, M. Tsimbrovska, V. Baroghel-Bouny, High performance concrete at elevated temperatures — an extensive experimental investigation on thermal, hygral and microstructure properties, in: P.C. Aïtcin, Y. Delagrave (Eds.), Proceedings of the International Symposium on High-Performance and Reactive Powder Concretes, Sherbrooke, Canada, 1998, pp. 127–143.
[29] M. Tsimbrovska, P. Kalifa, D. Quenard, J.F. Daïan, High performance concrete at elevated temperature: Permeability and microstructure, in: M. Livolant (Ed.), Transactions of the 14th International Conference on Structural Mechanics in Reactor Technology, Lyon, France 5, (1997) 475–482.
[30] E. Garboczi, K. Snyder, J. Douglas, M. Thorpe, Geometrical percolation threshold of overlapping ellipsoids, Phys. Rev. E: Stat. Phys., Plasmas, Fluids, Relat. Interdiscip. Top. 52 (1995) 819–828.
[31] J.J. Kollek, The determination of the permeability of concrete to oxygen by the Cembureau method, a recommendation, Mater. Struct. 22 (1989) 225–230.
[32] C. Gallé, J.-F. Daïan, Gas permeability of unsaturated cement-based materials: Application of a multi-scale network model, Mag. Concr. Res. 52 (2000) 251–263.
[33] L.J. Klinkenberg, The determination of porous media to liquids and gases, API Drill. Prod. Pract., (1941) 200–213.
[34] M. Tsimbrovska, Dégradation des bétons à hautes performances soumis à des températures élevées, Thèse de doctorat, Université de Grenoble, 1998.
[35] A.J. Katz, A.H. Thompson, A quantitative prediction of permeability in porous rocks, Physical Review B: Condensed Matter and Materials Physics 24 (1986) 8179–8181.
[36] N. Martys, E.J. Garboczi, Length scale relating the fluid permeability and electrical conductivity in random two-dimensional porous media, Physical Review B: Condensed Matter and Materials Physics 46 (1992) 6080–6090.
[37] E. Charlaix, E. Guyon, S. Roux, Permeability of a random array of fractures of widely varying apertures, Transp. Porous Media 2 (1987) 31–43.
[38] D. Quenard, Traité de physique du bâtiment: Partie G3, 1995, pp. 623–647.
[39] J.C. Maxwell-Garnett, Philos. Trans. R. Soc. London, Ser. B 205 (1906) 237.
[40] D.A.G. Bruggeman, Ann. Phys. (Leipzig) 24 (1935) 636.
[41] D.C. Maxwell, A Treatise on Electricity and Magnetism, third ed., Dover, New York, 1954.
[42] Z. Hashin, S. Shtrikman, A variational method of the theory of effective magnetic permeability of multiphase materials, J. Appl. Phys. 33 (1962) 3125.
[43] S. Kirpatrick, Classical transport in disordered media: Scaling and effective medium theories, Phys. Rev. Lett. 27 (1987) 1722.